2025 年宁波大学
曹光彪研究生科研成果奖

评审材料

学　　号 _____

申 报 人 _____

学　　院 _____

专业名称 _____

博士生/硕士生 _____

目 录

Self-Powered Piezoelectric and Thermoelectric Energy Simultaneous Extraction Interface Circuit Based on Double Stack Resonance

Xiudeng Wang, Yinshui Xia, Ge Shi, Huakang Xia, Yidie Ye, *Member, IEEE*, and Zhidong Chen

***Abstract*—A hybrid self-powered synchronous electric charge extraction (HSP-SECE) interface circuit based on double stack resonance is presented in this paper. The proposed HSP-SECE interface circuit can simultaneously extract energy from piezoelectric transducer (PZT) and thermoelectric generator (TEG) when the peak open-circuit voltage of the PZT is detected by passive peak detector. The output power of the proposed interface circuit can reach three times of that of full-bridge rectifier circuit at the maximum power point, and the maximum efficiency of harvesting thermoelectric energy can reach 76% at 200 mV of the open-circuit voltage of the TEG. The simulation and experimental results show the superiority of the HSP-SECE circuit.**

***Index Terms*—Double stack resonance, energy harvesting, piezoelectric transducer (PZT), self-powered, thermoelectric generator (TEG).**

I. Introduction

As a basic component of the Internet of Things (IoT), wireless sensor network (WSN) nodes have been widely used in wearable devices, consumer electronics, and environmental monitoring. However, traditional battery-powered methods for WSN nodes have become an important obstacle to the development of WSNs. According to the new IoT technical standard published by the third Generation Partnership Project (3GPP) organization, the battery-powered life of WSN nodes under normal operation should be more than ten years [1]. Therefore, harvesting environmental energy is considered as one of the effective methods to overcome this challenge [2].

Piezoelectric energy harvesting (PEH) is one of the promising techniques that can scavenge energy from ambient vibration sources. With its electromechanical coupling characteristic, a piezoelectric element can generate electricity when strain is produced. Since the deformation in a vibrating structure is alternating, the generated electricity is also alternating [3]. Therefore, an interface circuit is needed between the piezoelectric transducer (PZT) and the load, which is of rectification, voltage regulation, and impedance matching [4]. The simplest interface circuit is a full-bridge rectifier (FBR) circuit, and many researchers have made their efforts in the optimization of the FBR and even implemented the circuit in complementary metal oxide semiconductor (CMOS) integration [5], [6]. However, its harvesting efficiency is low because the parasitic capacitance in the piezoelectric element causes a phase difference between the voltage and current and hence reactive power [7], [8].

Therefore, a variety of nonlinear energy extraction circuits have been presented to improve the energy harvesting efficiency. Lefeuvre *et al.* [9]–[11] proposed a parallel synchronized switch harvesting on inductor (P-SSHI) circuit, a synchronous electric charge extraction (SECE) circuit, and a series synchronized switch harvesting on inductor (S-SSHI) circuit. These circuits can effectively increase the harvesting efficiency, but require additional circuits to control the switches. Based on the S-SSHI circuit, Liang and Liao [3] proposed a self-powered synchronized switch harvesting on inductor (SP-SSHI) circuit. Compared to the FBR circuit, its maximum output power can increase by 200%. Based on the SECE circuit, Shi *et al.* [12] put forward a self-powered efficient SECE (SP-ESECE) circuit and its harvesting efficiency can reach up to 85.1%. Eltamaly and Addoweesh [13] proposed a self-powered synchronized switch harvesting on inductor (SP-SSHI) circuit developed from the P-SSHI circuit, which has 10% efficiency increase compared to the circuit in [3]. However, the reported circuits require large inductor to achieve good performance, which significantly increase the system volume. Although a flipping-capacitor rectifier was proposed to flip voltages using on-chip capacitors in [14], it is designed for high-frequency (>100 kHz) ultrasonic energy transfer applications but does not work for PZTs with large parasitic capacitance C_p [15].

Thermoelectric energy harvesting circuit mainly includes inductive boost converter and charge pump (CP) circuit. The main challenge of thermoelectric energy harvesting is that the open-circuit voltage of thermoelectric generator (TEG) is low, such as 236∼265 mV at the temperature difference of 5 °C [16]. The

Manuscript received February 12, 2019; revised April 27, 2019; accepted June 18, 2019. Date of publication July 9, 2019; date of current version February 10, 2020. This work was supported in part by the National Natural Science Foundation of China under Grant U1709218, Grant 61601429, Grant 61771268, and Grant 61801253 and in part by the K. C. Wong Magna Fund in Ningbo University. *(Corresponding author: Xiudeng Wang.)*

X. Wang, Y. Xia, H. Xia, Y. Ye, and Z. Chen are with the Faculty of Electrical Engineering and Computer Science, Ningbo University, Ningbo 315211, China (e-mail: 1611082572@nbu.edu.cn; xiayinshui@nbu.edu.cn; xiahuakang@nbu.edu.cn; yeyidie@nbu.edu.cn; 1701082016@nbu.edu.cn).

G. Shi is with the College of Mechanical and Electrical Engineering, China Jiliang University, Hangzhou 310018, China (e-mail: shige@cjlu.edu.cn).

Color versions of one or more of the figures in this paper are available online at http://ieeexplore.ieee.org.

Digital Object Identifier 10.1109/TIE.2019.2926047

main limitations, indeed, come from the threshold voltage of diodes and pass transistors and the low transistor channel conductivity due to the low supply voltage [17]. Some researchers have proposed different methods, such as precharging output capacitors, adding mechanically assisted switches, and using external clocks or transformer startup circuits [18]. Das *et al*. [19] proposed a power-on-reset based self-starter with 2 nW quiescent power for thermoelectric energy harvester, which achieves a self-startup TEG voltage of 220 mV and a peak conversion efficiency of 76%. Yi *et al*. [20] used three-stage CP scheme employing a differential bootstrapped ring-VCO. The circuit has the efficiency of 38.8% at an input voltage of 150 mV and 45% at an input voltage of 200 mV. The CP circuit proposed by Kim *et al*. used dynamic body biasing and adaptive dead-time for efficiency improvement, which has an efficiency of 34% at an input voltage of 180 mV and 72.5% at an input voltage of 450 mV [21].

In order to harvest more energy, researchers have proposed some multisource harvesting circuits [22]–[25]. Lorenz *et al*. [22] presented a cooperative power harvesting scheme, collecting power from two or more independent ambient energy sources into a single nonlinear component. It is shown that the interaction of uncorrelated signals in a nonlinear device can greatly improve harvested power, but the conversion efficiency of the harvester is still low. Hsieh *et al*. [23] proposed a hybrid energy harvesting circuit in which both piezoelectric energy and solar energy are stored in a storage capacitor, and then an inductive boost circuit is used to power the load. However, the structure can only extract energy from energy source at higher open-circuit voltage. Yuk *et al*. [24] proposed a dual-source energy-harvesting interface circuit, which can harvest energy from both the PZT and the TEG. Yoon *et al*. [25] proposed a double pile-up resonance energy harvesting circuit that efficiently and simultaneously extracts energy from the PZT and the TEG. However, these circuits use an active control circuit module, which requires external power supply to start up the circuit.

In this paper, a hybrid self-powered SECE (HSP-SECE) interface circuit for harvesting dual-source energy is proposed. The proposed interface circuit can harvest both piezoelectric and thermoelectric energies simultaneously by double stack resonance.

This paper is organized as follows. In Section II, the circuit models of the PZT and the TEG, as well as the working principle of the FBR and the SECE circuits are introduced. In Section III, the architecture, working principle, and simulation analysis of the proposed interface circuit are described. In Section IV, the experimental results are provided. Section V concludes this paper.

II. Principles of Energy Harvesting

A. Equivalent Model of the PZT

Fig. 1(a) shows the coupled model of the PZT [8]. In the mechanical domain, V_S represents the external excitation force, L_M represents the mechanical mass, C_K is the mechanical stiffness, and R_S takes into account the mechanical damping. In the electrical domain, C_p represents the parasitic capacitance of the PZT. When the excitation is sinusoidal vibration, the vibration excitation of the PZT is modeled as a sinusoidal current source I_P in parallel with parasitic capacitance C_P and resistor R_P, as shown in Fig. 1(b) [26], [27].

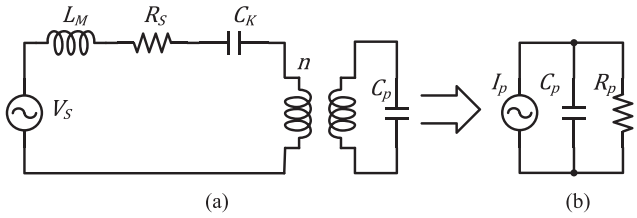

Fig. 1. PZT models. (a) Equivalent circuit model of the PZT. (b) Simplified circuit model under resonance conditions.

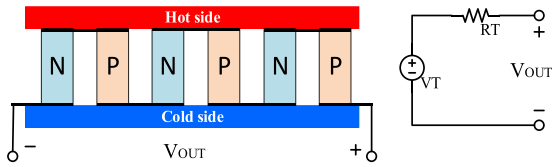

Fig. 2. Equivalent circuit of the TEG.

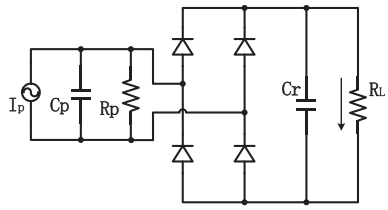

Fig. 3. Circuit of the FBR.

B. Equivalent Model of the TEG

Fig. 2 shows the structure of a typical TEG device. It consists of small legs of *P*- and *N*-type materials that are electrically connected in series. When a temperature difference is applied on two sides of the TEG, an open-circuit voltage between its two terminals is built because of the *Seebeck effect* [28]. In the literature, TEGs are mostly used under constant temperature gradient conditions. Moreover, the influence of the internal contact thermal resistance is usually neglected. Under these conditions, the TEG can be modeled as an equivalent constant voltage source in series with an equivalent internal resistance [29].

C. Theoretical Analysis of the FBR

The FBR circuit is used to convert the alternating current (ac) of the PZT output into direct current (dc), as shown in Fig. 3. R_L is the equivalent resistance as the actual load, and the storage capacitance of C_r is much larger than the parasitic capacitance C_p of the PZT in order to reduce the output voltage ripple. When the open-circuit voltage V_{oc} of the PZT is greater than the load voltage V_{RL}, the rectifier bridge is turned ON and the energy stored in the PZT can be transferred to the load. Otherwise, the rectifier diodes are turned OFF.

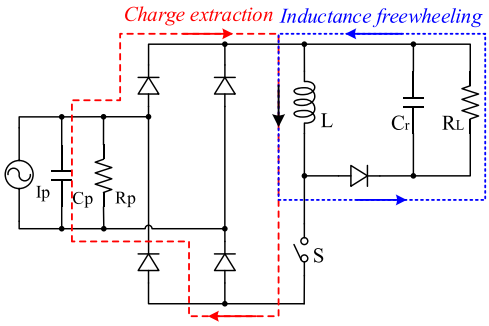

Fig. 4. Circuit of the SECE.

The output power of the FBR can be expressed as follows [30]:

$$P_{\mathrm{FBR}} = f2\int_0^{\frac{T_0}{2}} V_{RL} I_{\mathrm{PZT}}\, dt = 2f\alpha V_{RL}\int_{\mu_1}^{\mu_M} du \tag{1}$$

where f is the vibration frequency of the PZT, T_0 is the vibration period, α is the force factor of the PZT, μ_M is the peak displacement of the PZT, whereas μ_1 is the displacement of the PZT when the open-circuit voltage of the PZT is equal to the load voltage. The relationship between μ_1 and μ_M can be expressed as

$$\mu_1 = \frac{2C_p V_{RL}}{\alpha} - \mu_M. \tag{2}$$

Hence, the output power of the FBR can also be expressed as

$$P_{\mathrm{FBR}} = 4fV_{RL}\left[\alpha\mu_M - C_p\left(2V_D + V_{RL}\right)\right]. \tag{3}$$

V_D is the forward conduction voltage drop of diode.

The maximum output power and the corresponding optimal load resistance can be expressed as

$$P_{\mathrm{FBR,\,max}} = fC_p\left(\frac{\alpha\mu_M}{C_p} - 2V_D\right)^2 \tag{4}$$

$$R_{\mathrm{op}} = \frac{1}{4fC_p}. \tag{5}$$

If V_D is ignored, there is

$$P_{\mathrm{FBR,\,max}} = f\frac{\alpha^2\mu_M^2}{C_p} \tag{6}$$

D. Theoretical Analysis of the SECE

Compared to the FBR circuit, the SECE circuit adds an inductor L, a switch S, and a freewheeling diode, as shown in Fig. 4. The working principle of the SECE is that the charge accumulated in the parasitic capacitance C_p is transferred to the load side using the energy storage characteristics of the inductor. During one cycle, the switch is turned OFF at most of the time, the PZT is at an open state, and the energy in the equivalent current source I_p is transferred to the capacitor C_p [31].

The ideal current and voltage waveforms of C_p are shown in Fig. 5. When the switch is turned OFF, the equivalent current source I_p charges C_p so that the voltage across the PZT continuously rises. When the voltage is at its peak, I_p becomes

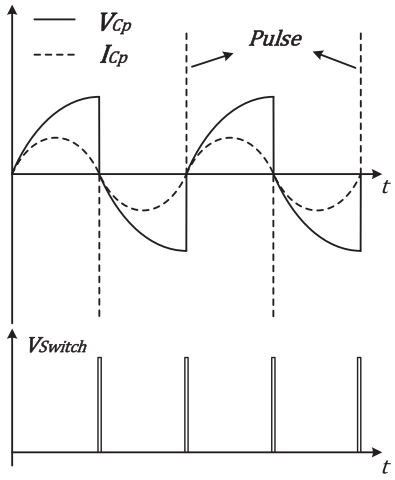

Fig. 5. Current and voltage of C_p and switching signal.

zero. At this time, the switch is turned ON so that the inductor L and capacitor C_p form a loop through the rectifying bridge, and hence the LC resonance occurs. After one-fourth resonance period, the switch is turned OFF immediately, and the accumulated energy on the C_p is completely transferred to the inductor. Meanwhile, the voltage quickly drops to zero. Then, L and C_p are disconnected, and the energy on the inductor can only be transferred to the load terminal through the freewheeling diode.

The LC_p loop resonance period can be expressed as

$$T_{LC_p} = 2\pi\sqrt{LC_p}. \tag{7}$$

Therefore, the turn-ON time of the switch can be expressed as

$$T_{S,\mathrm{on}} = \frac{1}{4}\,T_{LC_p} = \frac{1}{2}\,\pi\sqrt{LC_p}. \tag{8}$$

Since C_p is small, the turn-ON time of the switch is very short. Hence, a narrow current pulse is generated on C_p when the inductor begins to extract the charge, as shown in Fig. 5.

The peak voltage of the PZT can be expressed as

$$V_{p,\max} = \frac{2\alpha u_M}{C_p}. \tag{9}$$

Therefore, when the voltage reaches the peak point, the charge and energy accumulated on the capacitance C_p can be, respectively, expressed as

$$Q = C_p\, V_{p,\max} \tag{10}$$

$$E_{\mathrm{Cp}} = \frac{1}{2}C_p\, V_{p,\max}^2 = \frac{2\alpha^2\mu_M^2}{C_p}. \tag{11}$$

The principle of the SECE is to transfer the energy accumulated on C_p to the load twice in each cycle. Therefore, the output power of SECE can be expressed as

$$P_{\mathrm{SECE}} = f2E_{\mathrm{Cp}} = 4f\frac{\alpha^2\mu_M^2}{C_p}. \tag{12}$$

According to the aforementioned analysis, the output power of the SECE circuit is constant, because the SECE periodically

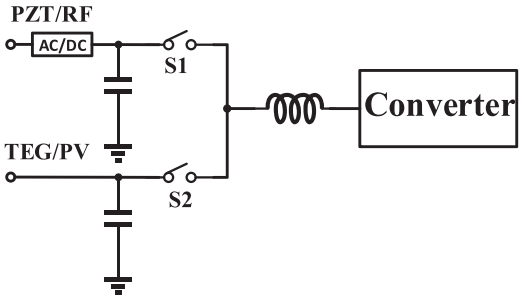

Fig. 6. Topological structure in [32] and [33].

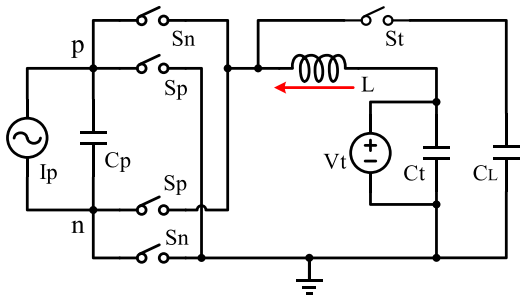

Fig. 7. Topological structure proposed in this paper.

extracts the energy accumulated on the parasitic capacitance through the *LC* resonance, which improves the energy harvesting efficiency and is not affected by the load. From (6) and (12), it can be found that the output power of the SECE is four times of the maximum output power of the FBR.

III. Proposed Interface Circuit

For multisource energy harvesting, the main issue is that the extracted energy from high power source may flow back to the lower power one. The simple solution is to set a diode between the energy transducer and the converter. However, this has twofold defects: on one hand, part of the harvested energy may be consumed on it; on the other hand, when the open circuit voltage of the energy transducer is lower than the diode threshold voltage, no energy can be harvested.

There were some circuits proposed for multisource energy harvesting [32]–[33]. The principle of the topology structure is shown in Fig. 6. Although it can harvest energy from multisources, it has two defects. First, it ignores the optimization of the rectifier circuit for ac energy, such as from piezoelectric or RF transducer. In the traditional practice, the ac energy supplied to the load requires a two-stage conversion consisting of a rectification and a ac–dc conversion, in which each stage of conversion consumes part of the harvested energy. Second, in order to prevent energy backflow, the switches S_1 and S_2 cannot be turned ON simultaneously. Hence, maximum power extraction of two energy sources cannot be achieved. For achieving the high efficiency of multisource energy harvesting, these switches must be precisely controlled. Thus, a switching control module with external power supply is required, which cannot implement the energy harvester with self-starting.

To solve this problem, a topological structure for simultaneously harvesting ac and dc energies is proposed in this paper. As shown in Fig. 7, C_p is the storage capacitance of the ac current source, and C_t is the storage capacitor of the dc voltage source. When the voltage of C_p reaches a positive (negative) peak, the energy stored in the capacitor also reaches a maximum value. At this time, the switch S_p (S_n) is turned ON, so that C_p, C_t, and the inductor form an *LC* resonant circuit with double stack resonance. After one-fourth *LC* resonant period, the energy accumulated on the capacitors C_p and C_t is transferred to the inductor. Then, the switch S_p (S_n) is immediately turned OFF while switch S_t is turned ON. The energy accumulated on the inductor is transferred to the load. Thereby the simultaneous extraction of ac energy at the maximum power point and dc energy is achieved.

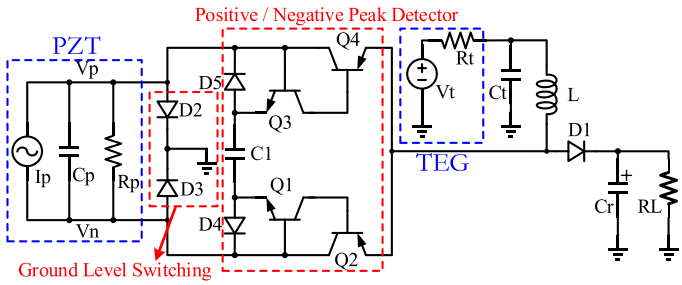

Fig. 8. Circuit of HSP-SECE.

Based on the aforementioned structure, by introducing a ground-level switching circuit and a positive/negative peak detector circuit, a HSP-SECE circuit with double stack resonance is implemented, as shown in Fig. 8, which can simultaneously harvest the energy from the PZT and the TEG. It mainly includes the TEG, the PZT, positive/negative peak detector, ground-level switching circuit, capacitors C_r, C_t, diode D_1, inductor L, and load resistor. Diode D_2 and transistor Q_2 are equivalent to switch S_p in Fig. 7, whereas diode D_3 and transistor Q_4 are equivalent to switch S_n, and diode D_1 is equivalent to switch S_t in Fig. 7. Diodes D_4 and D_5, transistors Q_1 and Q_3, and capacitor C_1 form a passive peak detector. Diodes D_2 and D_3 are turned ON in the positive/negative half cycle, respectively, so that the higher voltage end of the PZT is connected to the ground. Transistors Q_2/Q_4 are turned ON at positive and negative peaks, respectively. The detail working principle is analyzed as follows.

A. Theoretical Analysis of Working Principle

Diodes D_2 and D_3 constitute a ground-level switching circuit connecting to the higher voltage end of the PZT to ground so that capacitors C_p and C_t and inductor L constitute a resonant circuit when the switch is turned ON. Positive/negative peak detector is to detect the peak of the open-circuit voltage. When the open-circuit voltage of the PZT reaches its peak, the switch Q_2 (or Q_4) is turned ON while capacitors C_p and C_t and inductor L form a resonant loop, so that the energy accumulated on capacitors C_p and C_t can be conveyed to inductor L, and then the energy is

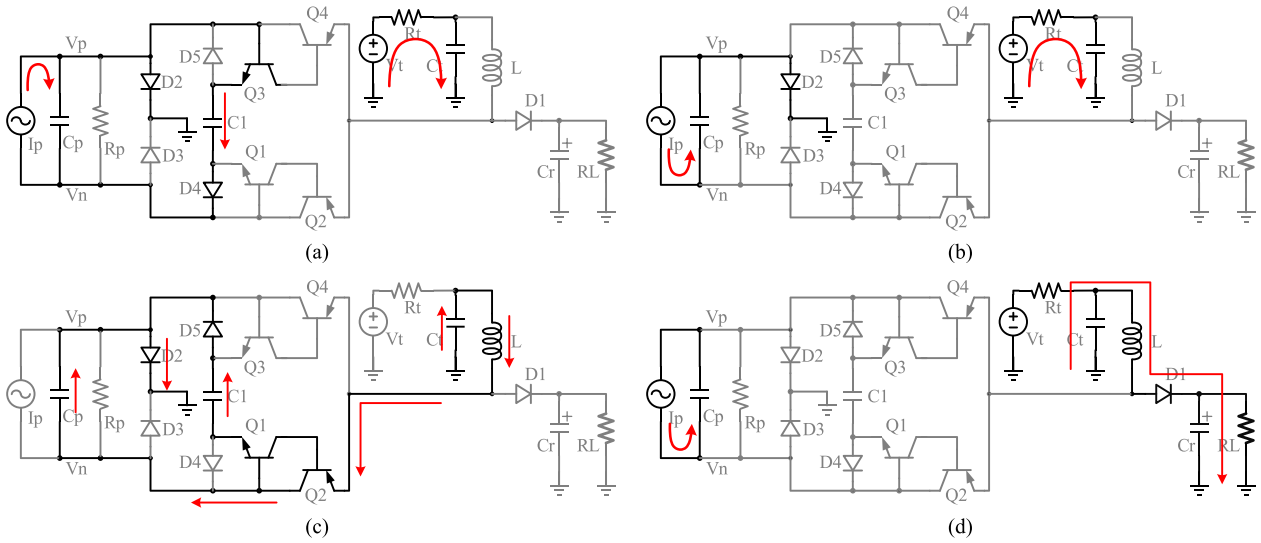

Fig. 9. Four phases within half of a vibration cycle. (a) Natural charging. (b) Current inversion. (c) Charge extraction. (d) Inductor freewheeling.

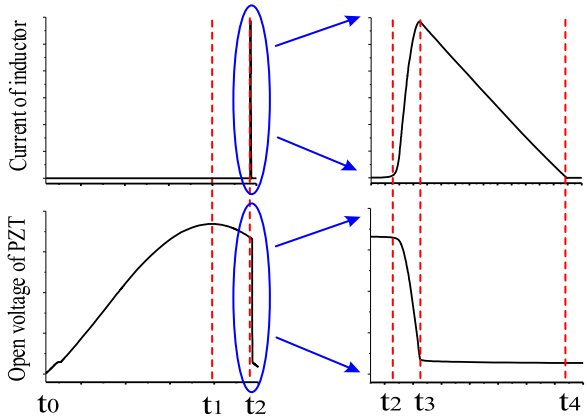

Fig. 10. Timing diagram of positive half cycle.

transferred to the load by freewheeling diode D_1. The specific working process is as follows.

In the positive half cycle, that is, V_p is higher than V_n, the circuit is mainly divided into four working phases, as shown in Fig. 9. The corresponding timing diagram is shown in Fig. 10, which includes the waveforms of the open-circuit voltage of the PZT and the current on the inductor at each working phase.

Natural charging $(t_0 - t_1)$*:* As shown in Fig. 9(a), the open-circuit voltage of the PZT gradually increases as the displacement increases. The parasitic capacitance C_p of the PZT and the capacitor C_1 in the peak detection circuit are always in the charged state. At the same time, the TEG also charges capacitor C_t. When the open-circuit voltage of the PZT reaches its maximum value, the equivalent current source I_p just reaches zero, whereas the voltages on C_p and C_1 both reach the maximum value. Then, the circuit starts to enter the second working phase.

When the open-circuit voltage of the PZT reaches an extreme value, the energy accumulated on C_p can be expressed as (11) and the voltage across capacitor C_1 also reaches the extreme

$$V_{C1,\max} = V_{p,\max} - V_{be} - V_D. \tag{13}$$

Hence, the energy accumulated on C_1 can be expressed as

$$E_{C1} = \frac{1}{2} C_1 V_{C1,\max}^2 = \frac{1}{2} c_1 (V_{p,\max} - V_{be} - V_D)^2. \tag{14}$$

Current inversion $(t_1 - t_2)$*:* As shown in Fig. 9(b), when the PZT begins to move in a reverse direction, the equivalent current source I_p starts to charge C_p inversely, so that the open-circuit voltage of the PZT starts to decrease. Due to the threshold voltage of diode D_5, the charge on C_1 is unable to be released and the voltage across C_1 remains unchanged. When the voltage across C_1 is higher than the open-circuit voltage of the PZT by the sum of the threshold voltage of transistor Q_1 and the turn-ON voltage drop of diode D_5, transistor Q_2 is turned ON while the voltage across capacitor C_t reaches its maximum value. Then, the circuit begins to enter the third working phase.

The energy accumulated on C_t can be expressed as

$$E_{Ct} = \frac{1}{2} C_t V_{Ct,\max}^2. \tag{15}$$

The open-circuit voltage of the PZT at this time is

$$V_p' = V_{C1,\max} - V_{be} - V_D = V_{p,\max} - 2V_{be} - 2V_D. \tag{16}$$

The corresponding energy accumulated on C_p is

$$E_{Cp}' = \frac{1}{2} C_p V_p'^2 = \frac{1}{2} C_p (V_{p,\max} - 2V_{be} - 2V_D)^2. \tag{17}$$

Hence, there is a phase lag, which can be expressed as θ

$$\theta = \cos^{-1}\left(\frac{V_{p,\max} - 2V_{be} - 2V_D}{V_{p,\max}}\right). \tag{18}$$

The energy loss caused by the phase lag can be expressed as

$$\Delta E_\theta = E_{Cp} - E_{Cp}' = \frac{1}{2} C_p V_{p,\max}^2 \sin^2\theta. \tag{19}$$

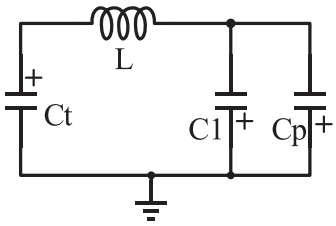

Fig. 11. Equivalent circuit of charge extraction.

It can be seen that the decrease of the extracted energy is closely related to θ. The efficiency of energy extraction can be expressed as

$$\eta = \frac{E_{Cp} - \Delta E_\theta}{E_{Cp}} = \cos^2 \theta. \tag{20}$$

The smaller the phase lag θ, the higher the efficiency of energy extraction.

Charge extraction $(t_2 - t_3)$*:* When the transistor Q_2 is turned ON, C_p, C_1, C_t, and L constitute an LC resonant loop, as shown in Fig. 9(c). If the turn-ON voltage drops of the transistor and diode are ignored, the equivalent circuit is shown in Fig. 11. It is noted that the high voltage terminals of C_1 and C_p are connected to ground, which is implemented through the ground-level switching circuit. Since the capacitance value of C_1 is much smaller than C_p, C_1 can be ignored. The equivalent circuit can be regarded as a single LC resonant circuit composed of C_p, C_t, and the inductor L, which is called double stack resonance. After one-fourth LC resonance period, the charges stacked on C_t and C_p are transferred to the inductor L. Therefore, the charge extracted by the inductor is increased compared to the pure SECE circuit.

The energy transferred to the inductor can be calculated as

$$E'_L = E'_{\mathrm{Cp}} + E_{Ct} + E_{C1}. \tag{21}$$

According to (21), compared to published self-powered PEH interface circuits, the HSP-SECE circuit can not only harvest E'_{Cp} but also simultaneously harvest thermoelectric energy E_{Ct} based on double stack resonance.

However, in the charge extraction process, both the diode and the transistor consume energy as long as there are currents flowing through them. As shown in Fig. 9(c), there are currents flowing through four devices, Q_2, D_2, Q_1, and D_5. However, the current through Q_2 and D_2 is much larger than that through Q_1 and D_5. Hence, the energy consumed by the former is much larger than the later. Assuming that the energy consumption by the former is considered and the turn-ON voltage drops of Q_2 and D_2 remain unchanged, the energy consumed in the charge extraction process can be expressed as

$$E_{\mathrm{CE,loss}} = \int (V_D + V_{\mathrm{CE}})\, I\,(t)\, dt\ . \tag{22}$$

Here V_D and V_{CE} represent the voltage drops across the diode and transistor, respectively.

Inductor freewheeling $(t_3 - t_4)$*:* After the energy on the capacitor C_1 is fully discharged, Q_2 is turned OFF. Through the freewheeling diode D_1, the inductor L and the load form a loop to transfer the energy accumulated on the inductor to the load, and the equivalent current source starts to charge the C_p inversely, as shown in Fig. 9(d). Then, the energy extraction of the positive half cycle is completed.

During the process of the inductor freewheeling, the components also consume energy. If the internal resistance of the inductor is neglected, the main energy loss causes from the freewheeling diode D_1 is

$$E_{\mathrm{IF,loss}} = \int V_D\, I\,(t)\, dt\ . \tag{23}$$

From another perspective, the conversion efficiency of the inductor freewheeling process can be simplified as

$$\eta_{\mathrm{IF}} = \frac{V_{\mathrm{out}}}{V_{\mathrm{out}} + V_D}\ . \tag{24}$$

From (24), it can be seen that the conversion efficiency increases with output voltage increase.

During the negative half cycle, the HSP-SECE circuit works in a similar way.

TABLE I
DATA OF THE COMPONENTS

Component	Value
I_p	300uA/20Hz
C_p	200nF
R_p	2MΩ
C_1	2.8nF
V_t	200mV
R_t	10Ω
C_t	100uF
L	0.5mH
C_r	200uF
RL	50kΩ

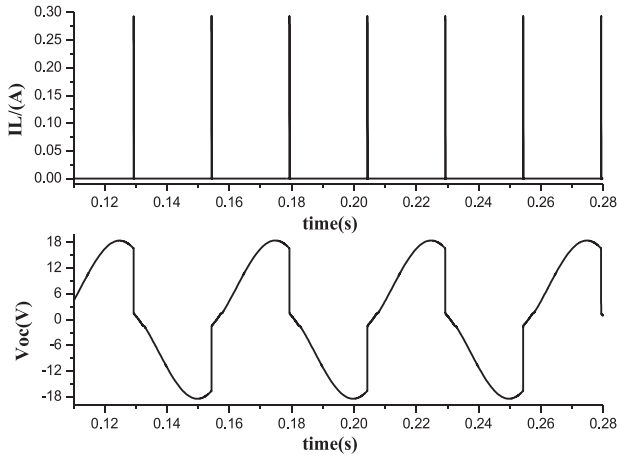

Fig. 12. Current of L and open-circuit voltage of PZT.

B. Simulation Analysis

The simulation of the proposed HSP-SECE circuit is performed. The parameters of the components used are shown in Table I. Fig. 12 shows the PZT open-circuit voltage and current through the inductor L. It can be seen that both the inductor current and the open-circuit voltage of the PZT are periodically

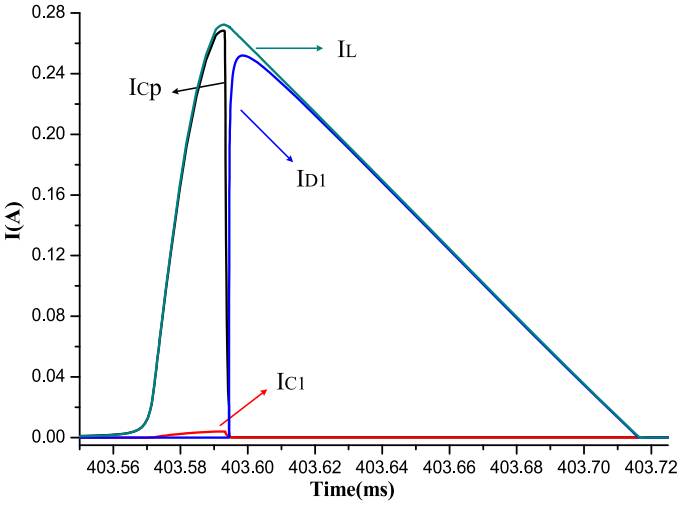

Fig. 13. Current waveforms of L, C_p, C_1, and D_1.

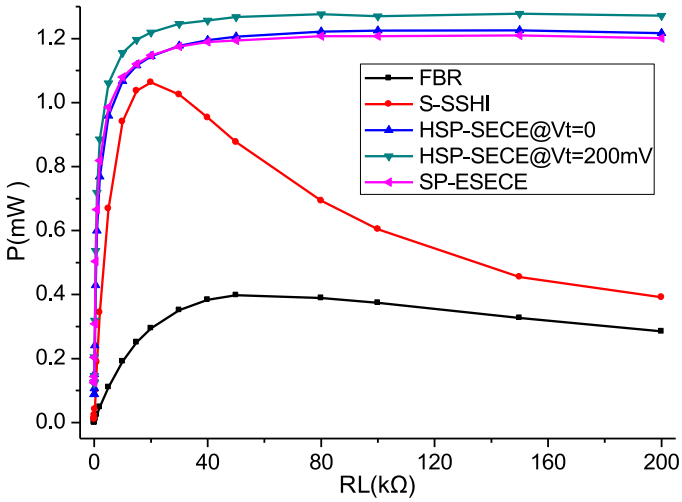

Fig. 14. Output power comparison of several circuits under the same excitation and different loads.

varied. When the inductor generates a current pulse, the open-circuit voltage of the PZT drops rapidly. It can be seen that there is a phase lag between the current pulse and the peak voltage of the PZT, which confirms (18).

In order to understand the energy extraction process of the HSP-SECE circuit, the relevant current waveform is zoomed in to observe the detail clearly at the instant of switching conduction. Fig. 13 shows the currents on inductor L, capacitors C_p and C_1, and freewheeling diode D_1, respectively. According to the previous theoretical analysis, before the current peak, it is the energy extraction process, whereas after the current peak, it is the inductor free-wheeling process. When the inductor current rises, the currents through capacitors C_p, C_1, and C_t have the same direction and the sum of the currents of the capacitors C_p and C_1 equals the inductor current, which confirms the analysis for Fig. 11 and in other words, the energy accumulated on capacitor C_1 can be recycled. As the inductor current reaches its peak, the currents of capacitors C_p and C_1 drop to zero. At this point, the energy extraction process ends. When the energy on the capacitor C_1 is completely released, the peak detector turns the switch (Q_2 or Q_4) OFF, and the circuit immediately enters the inductor free-wheeling process. Then, the current of diode D_1 rises quickly to the inductor current, which means that the energy extraction is completed. However, near the peak of the diode current, there is a difference between the inductor current and the diode current. This is that the circuit uses a passive peak detector to control the switching transistor Q_2 (or Q_4), so that the transistor cannot be quickly disconnected, which leads to partial current leakage.

C. Comparative Analysis

In order to compare the load dependence of several different circuit structures and the advantages of each type of the circuits, the HSP-SECE circuit proposed in this paper and the published circuits are simulated. The simulation is based on the equivalent circuit model shown in Fig. 1 and the value of the load resistance is adjusted while the parameters I_p, C_p, R_p, and load capacitance C_r keep constant. The constant parameters are the same as Table I. Since a purely resistive load is used, according to *Ohm's law*, the output power varies with the load, which also means that the output power changes with the output voltage. Fig. 14 shows the output power of the FBR, S-SSHI circuits in [3], SP-ESECE circuit in [12], and the proposed HSP-SECE circuit at $V_t = 0$ mV and $V_t = 200$ mV, respectively. From the simulation results, the maximum output power of the HSP-SECE, SP-ESECE, and S-SSHI circuits are 3.05 ($V_t = 0$ mV), 3, and 2.64 times of that of the FBR circuit, respectively.

From Fig. 14, it can be seen that the output power of the S-SSHI and SP-ESECE circuits is higher than that of the FBR circuit in the entire load range. It also can be seen that when the load resistance is lower than 20 kΩ, the output power is small, and increases as the load value increases, which is in accordance with the description of (24). However, when the load resistance exceeds 20 kΩ, the output power of the S-SSHI circuit begins to decrease significantly as the load increases, whereas the output power of the SP-ESECE and the HSP-SECE circuits remains almost unchanged. This also proves that the harvesting efficiency of the SECE circuit is hardly affected by the load.

When the load is higher than 50 kΩ, the output power of the HSP-SECE circuit is higher than that of the SP-ESECE circuit even when the TEG open-circuit voltage is 0 mV, and it is significantly higher than that of the S-SSHI circuit. For the HSP-SECE circuit, when the TEG open-circuit voltage is 200 mV, the output power is significantly higher than that when the TEG open-circuit voltage is zero. It shows that the HSP-SECE circuit can effectively extract the thermoelectric energy even if the open-circuit voltage of the TEG is as low as 200 mV.

In order to test the advantages of the HSP-SECE circuit for harvesting thermoelectric energy, the circuit under the same piezoelectric excitation with different output voltages is simulated. The simulation results are shown in Fig. 15. Three sets of data are measured, corresponding to TEG's open circuit

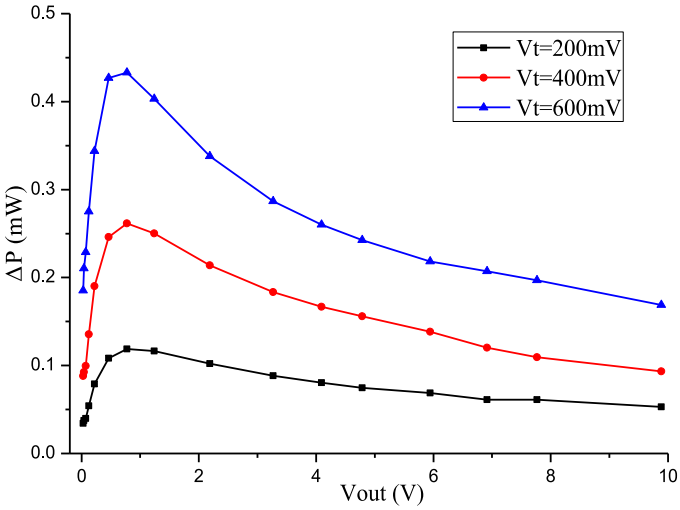

Fig. 15. ΔP under different output voltage.

voltages of 200, 400, and 600 mV, respectively. In the figure, the abscissa represents the effective value of the output voltage of the circuit, whereas the ordinate ΔP stands for the difference between the output power under the specific V_t and the output power when $V_t = 0$ mV. From Fig. 15, it can be seen that when the output voltage is very low, ΔP is small, which means that the advantage of the hybrid energy harvester is not obvious. This is mainly that most of the energy is consumed by the freewheeling diode when the output voltage is low, which is consistent with (24). Therefore, the output power will gradually increase as the output voltage increases. When the output voltage is about 1 V, ΔP reaches its maximum value. However, as the output voltage increases, ΔP begins to decrease slowly. This is that during the inductor freewheeling process, as the output voltage increases, the anode voltage of the freewheeling diode gradually increases, and the positive voltage of the capacitor C_t increases. Therefore, the current charged by the TEG to capacitor C_t is reduced so that the output power of the TEG slightly decreases.

IV. Experimental Work

In order to verify the aforementioned theoretical and simulation analyses, experimental platform is set up, as shown in Fig. 16. The experimental system is composed of a function signal generator, an oscilloscope, a PZT, a dc source, a power amplifier, a vibrating table, a TEG device, and the HSP-SECE energy harvesting circuit. The sinusoidal signal generated by the signal generator is used to control the vibrating table after being enhanced by the power amplifier. One end of the PZT is tightly fixed with a metal mass, and the other end is fixed on the vibrating table. When the vibrating table works, due to the inertia of the metal mass, a relative displacement between two ends of the PZT occurs so that the PZT deforms accordingly and generates an ac signal. Before connecting the circuit, the vibration frequency and amplitude need to be adjusted by the signal generator and power amplifier. Only when the vibration frequency is adjusted to the resonance state, the open circuit

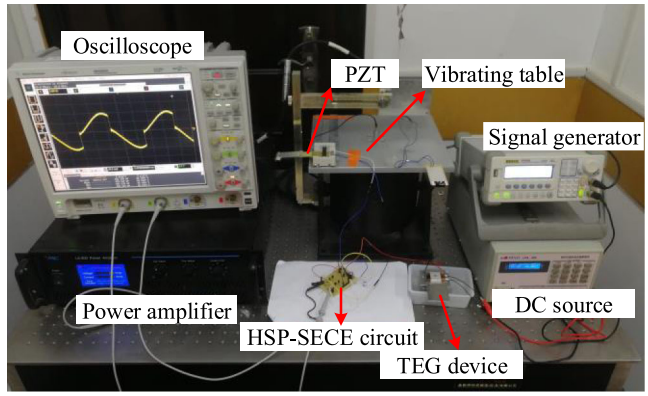

Fig. 16. Experimental setup.

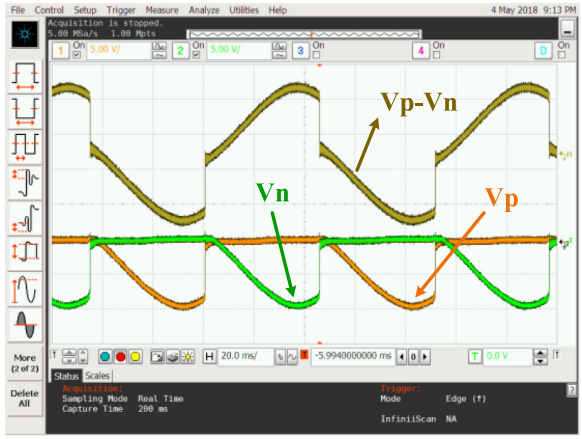

Fig. 17. Experimental waveforms.

voltage of the PZT reaches the maximum. The TEG device consists of a TEG, a container filled with cold water, a positive temperature coefficient (PTC) heating sheet and a heat sink. The heated surface of the TEG is attached to the PTC heating sheet, whereas the cold surface is placed on the heat sink, which is placed in the cold water container. The PTC heating sheet is powered by a dc source. Adjusting the output voltage of the dc source can control the temperature of the heating sheet, which can change the temperature difference across the TEG. When the output voltages of the TEG and PZT are stable, they are connected to the circuit for testing.

Fig. 17 shows the voltage waveforms measured by the oscilloscope, which corresponds to the voltage waveforms at both ends of the PZT and the open-circuit voltage waveforms, respectively. When the PZT's open-circuit voltage reaches its peak, it rapidly drops to zero after a delay, the voltage starts to reverse, and the PZT is at an open-circuit state. Therefore, the PZT's open-circuit voltage begins to increase with the increase of the PZT's displacement, which is in line with the simulation results.

Fig. 18 shows the measured output power of the HSP-SECE circuit when the excitation frequency of the PZT is maintained at 22 Hz and the load resistance remains at 150 kΩ. The temperature difference between the two sides of the TEG and the PZT vibration amplitude is gradually increased. It can be seen

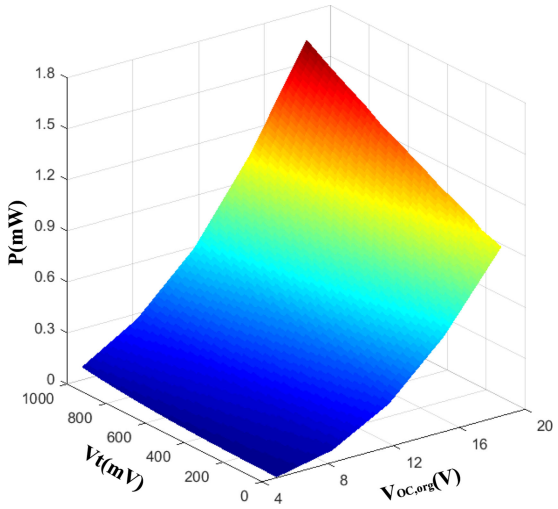

Fig. 18. Output power at different open-circuit voltages of TEG and PZT (with $C_t = 100$ μF).

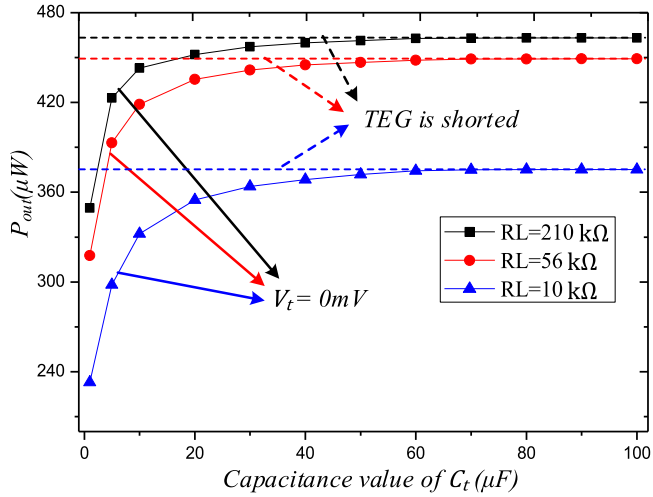

Fig. 19. When $V_t = 0$ mV, the output power changes with C_t.

that the output power of the circuit is positively correlated with the amplitude of the PZT and the temperature difference of the TEG. When the amplitude of the PZT remains unchanged, the output power tends to increase linearly with the increase of the open circuit voltage of the TEG. When the temperature difference between the two ends of the TEG remains unchanged, the output power increases exponentially with the increase of the original open-circuit voltage of the PZT. This indicates that the HSP-SECE circuit can harvest energy from the PZT and the TEG at the same time. Furthermore, it can be seen that as the open-circuit voltage of the PZT increases, the curvature of the curve increases significantly with the thermoelectric voltage increase, which means that as the amplitude of the vibration increases, the harvesting efficiency of the thermoelectric energy can be enhanced.

In order to verify whether TEG has an effect on the efficiency of PEH, we tested the output power of the HSP-SECE circuit when the open-circuit voltage of the TEG was 0 V and the TEG was shorted (equivalent to an SECE circuit for PEH) when $V_{OC,\text{org}} = 13$ V remained unchanged, as shown in Fig. 19. As illustration, when C_t is small, the TEG significantly impair the efficiency of PEH. While $C_t \geq 60$ uF, the output power of the circuit is almost the same as that of the SECE circuit. Therefore, in practical applications, it is necessary to select a larger value of C_t, so that the efficiency of PEH is not affected by the TEG.

Table II summarizes comparison results among the HSP-SECE circuit and those state-of-the-art circuits, which are for PEH in [3] and [12] based on S-SSHI and SECE, respectively, thermoelectric energy harvesting in [20] and [21] based on charge-pump and both piezoelectric energy and thermoelectric energy harvesting in [24] and [25].

Compared with those single energy harvesting methods, the HSP-SECE circuit is of comparative advantages. In terms of PEH, the harvesting efficiency of the HSP-SECE can be up to three times of that of the FBR circuit with only a 0.5-mH inductor though the maximum efficiency of the S-SSHI in [3] can also reach three times of the FBR circuit with a 47-mH inductor and under optimal load. For thermoelectric harvesting, on one hand, the harvesting efficiency of the HSP-SECE is as high as 76% at input voltage 200 mV, whereas the efficiencies from the state-of-the-art circuits in [20] and [21] are 45% at input voltage 200 mV and 72.5% at input voltage 450 mV, respectively, and their harvesting efficiencies are rapidly decreased as the input voltages decrease; on the other hand, the minimum starting voltage of the HSP-SECE circuit can be as low as 50 mV, whereas that in [20] and [21] is 150 mV.

In terms of dual energy-source harvesting, from Table II, it can be seen that the HSP-SECE circuit not only can simultaneously harvests piezoelectric and thermoelectric energies but also is self-powered. The circuits in [24] and [25] from the same research group can also simultaneously harvest piezoelectric and thermoelectric energies. It can be seen that the maximum efficiencies of thermoelectric harvesting for both the HSP-SECE circuit and the circuit in [25] have similar value. Although the PEH efficiency of the HSP-SECE is only three times of that of the FBR, whereas the circuits in [24] and [25] can be as high as 4.22 and 14.52 times, respectively, the latter requires an external power supply and hence the power loss of the circuit is hard to be calculated. Once the battery is exhausted, the harvester will be paralyzed and unable to restart. In addition, since the circuits in [24] and [25] are implemented in CMOS process, the piezoelectric energy at low open-circuit voltage can be harvested, so that the maximum output power can only be as low as 87 and 16 μW, respectively. The output power of the HSP-SECE circuit is less affected by the load size and maintains a high harvesting efficiency over a wide load range. However, the circuit in [25] can maintain a high harvesting efficiency only in the optimal load region. If the load is too large or too small, the efficiency will be significantly reduced. The circuit in [25] contains a boost circuit, which can separately harvest thermoelectric energy. The circuit proposed in this paper can harvest piezoelectric energy separately, but it is not possible to separately harvest thermoelectric energy.

TABLE II
PERFORMANCE COMPARISON

Publication	TIE 2012[3]	JIMSS 2016[12]	TCS II 2018 [20]	JSSC 2015[21]	ISSCC 2014[24]	JSSC 2018[25]	This Work
Input Sources	PZT	PZT	TEG	TEG	PZT+TEG	PZT+TEG	**PZT+TEG**
PZT	N/A	N/A	N/A	N/A	N/A	PPA-1001	**PPA-1011**
Features	S-SSHI	SECE	Charge-Pump	Charge-Pump	Pile-Up Resonance	Double Pile-Up Resonance	**Double Stack Resonance**
Self-Power	YES	YES	YES	YES	NO	NO	**YES**
Inductor	47mH	1mH	N/A	N/A	N/A	0.68mH	**0.5mH**
Boost to $FBR_{(max)}$	3× @1.5mW	3× @2mW	N/A	N/A	4.22× @87μW	14.52× @16μW	**3× @1mW**
Peak efficiency of TEG	N/A	N/A	38.8%@150mV 45%@200mV	34%@ 180mV 72.5%@450mV	N/A	75%(booster)	**76%@200mV**
Startup voltage of TEG	N/A	N/A	150mV	150mV	500mV	100mV	**50mV**
Frequency/Hz	30	50	N/A	N/A	100	140	**22**

V. CONCLUSION

In this paper, the method to simultaneously harvest the energy from PZT and TEG was studied. An HSP-SECE circuit based on double stack resonance was proposed. Theoretical analysis, simulation, and experimental results showed that an HSP-SECE circuit can effectively harvest both piezoelectric and thermoelectric energies simultaneously, and maintain a high efficiency for ultralow voltage thermoelectric energy harvesting. However, it should be pointed out that for the proposed circuit, when the open-circuit voltage of the TEG was zero, the internal resistance of the TEG might consume a small part of the power harvested from the PZT.

REFERENCES

[1] J. Gozalvez, "New 3GPP standard for IoT [mobile radio]," *IEEE Veh. Technol. Mag.*, vol. 11, no. 1, pp. 14–20, Mar. 2016.

[2] V. Raghunathan, S. Ganeriwal, and M. Srivastava, "Emerging techniques for long lived wireless sensor networks," *IEEE Commun. Mag.*, vol. 44, no. 4, pp. 108–114, Apr. 2006.

[3] J. Liang and W. Liao, "Improved design and analysis of self-powered synchronized switch interface circuit for piezoelectric energy harvesting systems," *IEEE Trans. Ind. Electron.*, vol. 59, no. 4, pp. 1950–1960, Apr. 2012.

[4] Y. Rao and D. P. Arnold, "An input-powered active AC/DC converter with zero standby power for energy harvesting applications," *IEEE Energy Convers. Congr. Expo.*, Sep. 2010, pp. 4441–4446.

[5] Y. Li, Z. Zhu, Y. Yang, and C. Zhang, "An ultra-low-voltage self-powered energy harvesting rectifier with digital switch control," *IEICE Electron. Express*, vol. 12, no. 3, Feb. 2015, Art. no. 20140921.

[6] A. L. F. Stein and H. F. Hofmann, "Autonomous wideband piezoelectric energy harvesting utilizing a resonant inverter," *IEEE Trans. Power Electron.*, vol. 32, no. 8, pp. 6178–6187, Aug. 2017.

[7] D. A. Sanchez, J. Leicht, F. Hagedorn, E. Jodka, E. Fazel, and Y. Manoli, "A parallel-SSHI rectifier for piezoelectric energy harvesting of periodic and shock excitations," *IEEE J. Solid-State Circuits*, vol. 51, no. 12, pp. 2867–2879, Dec. 2016.

[8] G. Shi, Y. Xia, X. Wang, L. Qian, Y. Ye, and Q. Li, "An efficient self-powered piezoelectric energy harvesting CMOS interface circuit based on synchronous charge extraction technique," *IEEE Trans. Circuits Syst. I, Reg. Papers*, vol. 65, no. 2, pp. 804–817, Dec. 2018.

[9] E. Lefeuvre and C. Richard, "High-performance piezoelectric vibration energy reclamation," in *Proc. SPIE—Int. Soc. Opt. Eng.*, Jul. 2004, vol. 5390, pp. 379–388.

[10] E. Lefeuvre, A. Badel, C. Richard, and D. Guyomar, "Piezoelectric energy harvesting device optimization by synchronous electric charge extraction," *J. Intell. Mater. Syst. Struct.*, vol. 16, no. 10, pp. 865–876, Oct. 2005.

[11] E. Lefeuvre, A. Badel, C. Richard, L. Petit, and D. Guyomar, "A comparison between several vibration-powered piezoelectric generators for standalone systems," *Sensors Actuators A, Phys.*, vol. 126, no. 2, pp. 405–416, Feb. 2006.

[12] G. Shi, Y. Xia, Y. Ye, L. Qian, and Q. Li, "An efficient self-powered synchronous electric charge extraction interface circuit for piezoelectric energy harvesting systems," *J. Intell. Mater. Syst. Struct.*, vol. 27, no. 16, pp. 2160–2178, Sep. 2016.

[13] A. M. Eltamaly and K. E. Addoweesh, "A novel self-power SSHI circuit for piezoelectric energy harvester," *IEEE Trans. Power Electron.*, vol. 32, no. 10, pp. 7663–7673, Oct. 2017.

[14] Z. Chen, M. Law, P. Mak, W. Ki, and R. P. Martins, "Fully integrated inductor-less flipping-capacitor rectifier for piezoelectric energy harvesting," *IEEE J. Solid-State Circuits*, vol. 52, no. 12, pp. 3168–3180, Dec. 2017.

[15] S. Du and A. A. Seshia, "A fully integrated split-electrode synchronized-switch-harvesting-on-capacitors (SE-SSHC) rectifier for piezoelectric energy harvesting with between 358% and 821% power-extraction enhancement," in *Proc. IEEE Int. Solid-State Circuits Conf.*, Feb. 2018, pp. 152–154.

[16] P. Spies, M. Pollak, and G. Rohmer, "Energy harvesting for mobile communication devices," in *Proc. 29th Int. Telecommun. Energy Conf.*, Sep. 2007, pp. 481–488.

[17] A. Richelli, S. Comensoli, and Z. M. Kovacs-Vajna, "A DC/DC boosting technique and power management for ultralow-voltage energy harvesting applications," *IEEE Trans. Ind. Electron.*, vol. 59, no. 6, pp. 2701–2708, Jun. 2012.

[18] Q. Liu, X. Wu, M. Zhao, L. Wang, and X. Shen, "30–300 mV input, ultra-low power, self-startup DC-DC boost converter for energy harvesting system," in *Proc. IEEE Asia Pacific Conf. Circuits Syst.*, Dec. 2012, pp. 432–435.

[19] A. Das, Y. Gao, and T. T. H. Kim, "A 220-mV power-on-reset based self-starter with 2-nW quiescent power for thermoelectric energy harvesting systems," *IEEE Trans. Circuits Syst. I, Reg. Papers*, vol. 64, no. 1, pp. 217–226, Jan. 2017.

[20] H. Yi, J. Yin, P. Mak, and R. P. Martins, "A 0.032-mm 2 0.15-V three-stage charge-pump scheme using a differential bootstrapped ring-VCO for energy-harvesting applications," *IEEE Trans. Circuits Syst. II, Express Briefs*, vol. 65, no. 2, pp. 146–150, Feb. 2018.

[21] J. Kim, P. K. T. Mok, and C. Kim, "A 0.15 V input energy harvesting charge pump with dynamic body biasing and adaptive dead-time for efficiency improvement," *IEEE J. Solid-State Circuits*, vol. 50, no. 2, pp. 414–425, Feb. 2015.

[22] C. H. P. Lorenz, S. Hemour, W. Liu, A. Badel, F. Formosa, and K. Wu, "Hybrid power harvesting for increased power conversion efficiency," *IEEE Microw. Wireless Compon. Lett.*, vol. 25, no. 10, pp. 687–689, Oct. 2015.

[23] Y. T. Hsieh, C. Fang, C. Su, H. Tsai, and Y. Juang, "A hybrid ambient energy harvesting integrated chip (IC) for the Internet of Things (IoT) and portable applications," in *Proc. 19th Int. Conf. Elect. Mach. Syst.*, Nov. 2016, pp. 1–4.

[24] Y. S. Yuk *et al.*, "23.5 An energy pile-up resonance circuit extracting maximum 422% energy from piezoelectric material in a dual-source energy-harvesting interface," in *Proc. IEEE Int. Solid-State Circuits Conf. Dig. Tech. Papers*, Feb. 2014, pp. 402–403.
[25] K. S. Yoon, S. W. Hong, and G. H. Cho, "Double pile-up resonance energy harvesting circuit for piezoelectric and thermoelectric materials," *IEEE J. Solid-State Circuits*, vol. 53, no. 4, pp. 1049–1060, Apr. 2018.
[26] G. K. Ottman, H. F. Hofmann, A. C. Bhatt, and G. A. Lesieutre, "Adaptive piezoelectric energy harvesting circuit for wireless remote power supply," *IEEE Trans. Power Electron.*, vol. 17, no. 5, pp. 669–676, Sep. 2002.
[27] M. Shim, J. Kim, J. Jeong, S. Park, and C. Kim, "Self-powered 30 μW to 10 mW piezoelectric energy harvesting system with 9.09 ms/V maximum power point tracking time," *IEEE J. Solid-State Circuits*, vol. 50, no. 10, pp. 2367–2379, Oct. 2015.
[28] M. Alhawari, B. Mohammad, H. Saleh, and M. Ismail, "A survey of thermal energy harvesting techniques and interface circuitry," in *Proc. IEEE 20th Int. Conf. Electron., Circuits, Syst.*, Dec. 2013, pp. 381–384.
[29] S. Siouane, S. Jovanović, and P. Poure, "Equivalent electrical circuit of thermoelectric generators under constant heat flow," in *Proc. IEEE 16th Int. Conf. Environ. Elect. Eng.*, Jun. 2016, pp. 1–6.
[30] L. Garbuio, M. Lallart, D. Guyomar, C. Richard, and D. Audigier, "Mechanical energy harvester with ultralow threshold rectification based on SSHI nonlinear technique," *IEEE Trans. Ind. Electron.*, vol. 56, no. 4, pp. 1048–1056, Apr. 2009.
[31] Y. Wu, A. Badel, F. Formosa, W. Liu, and A. E. Agbossou, "Piezoelectric vibration energy harvesting by optimized synchronous electric charge extraction," *J. Intell. Mater. Syst. Struct.*, vol. 24, no. 12, pp. 1445–1458, Aug. 2013.
[32] S. Bandyopadhyay and A. P. Chandrakasan, "Platform architecture for solar, thermal, and vibration energy combining with MPPT and single inductor," *IEEE J. Solid-State Circuits*, vol. 47, no. 9, pp. 2199–2215, Sep. 2012.
[33] G. Chowdary, A. Singh, and S. Chatterjee, "An 18 nA, 87% efficient solar, vibration and RF energy-harvesting power management system with a single shared inductor," *IEEE J. Solid-State Circuits*, vol. 51, no. 10, pp. 2501–2513, Oct. 2016.

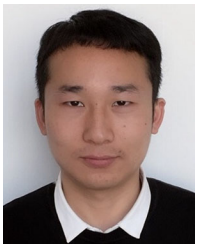

Xiudeng Wang was born in Xinyang, China, in 1992. He received the B.E. degree in communication engineering in 2016 from Ningbo University, Ningbo, China, where he is currently working toward the M.S. degree in circuits and systems.

His research interests include energy harvesting technique, sensors and measuring technology, ultralow power integrated circuits design, as well as embedded system.

Yinshui Xia received the B.S. degree in physics and the M.S. degree in electronic engineering from Hangzhou University, Hangzhou, China, in 1984 and 1991, respectively, and the Ph.D. degree in electronic engineering from Edinburgh Napier University, Edinburgh, U.K., in 2003.

He was a Visiting Scholar with King's College London, London, U.K., in 1999 and a Research Assistant and an Enterprise Fellow with Edinburgh Napier University, from 2000 to 2005. He is currently a Professor with the Faculty of Electrical Engineering and Computer Science, Ningbo University, Ningbo, China. His research interests include energy harvesting technique, low-power digital circuit design, logic synthesis and optimization, and system on chip design.

Ge Shi received the B.E. degree in electrical engineering and automation and the M.S. degree in detection technology and automation from China Jiliang University, Hangzhou, China, in 2004 and 2010, respectively, and the Ph.D. degree in micro-nano information system from Ningbo University, Ningbo, China, in 2018.

He is currently a Senior Experimentalist with China Jiliang University. His current research interests include energy harvesting technique, sensors and measuring technology, ultralow power integrated circuits design, as well as embedded system.

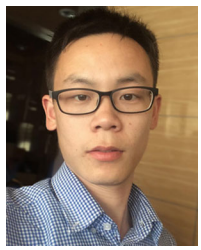

Huakang Xia received the B.S. degree in aircraft design and engineering and the Ph.D. degree in instrument science and technology from the Nanjing University of Aeronautics and Astronautics, Nanjing, China, in 2012 and 2017, respectively.

He is currently a Lecturer with the Faculty of Electrical Engineering and Computer Science, Ningbo University, Ningbo, China. His current research interests include energy harvesting technique ultralow power circuit design, as well as embedded system.

Yidie Ye (M'18) received the B.S., M.S., and Ph.D. degrees in microelectronics from Zhejiang University, Hangzhou, China, in 2007, 2010, and 2012, respectively.

She is currently a Lecturer with the Faculty of Electrical Engineering and Computer Science, Ningbo University, Ningbo, China. Her current research interests include low-power circuit design and optimization.

Zhidong Chen received the B.S. degree in electronic and information engineering and the M.S. degree in electronic circuit and system from Hangzhou Dianzi University, Hangzhou, China, in 2011 and 2014, respectively. He is currently working toward the Ph.D. degree in micro-nano information system with Ningbo University, Ningbo, China.

He is currently a Lecturer with Zhejiang Business Technology Institute, Ningbo, China. His research interests include energy harvesting technique and sensors and measuring technology.

宁波大学 NINGBO UNIVERSITY

文献检索报告
SCI 收录

宁波大学图书馆与信息中心 NBULIB 报告编号：20203600OZ190740-0

经检索 科学引文索引（Science Citation Index Expanded） 数据库，查晓婧 提供的如下论文被 SCI 收录，收录记录简要信息摘选如下：

出版物类型: J
作者: Wang, XD (Wang, Xiudeng); Xia, YS (Xia, Yinshui); Shi, G (Shi, Ge); Xia, HK (Xia, Huakang); Ye, YD (Ye, Yidie); Chen, ZD (Chen, Zhidong)
标题: Self-Powered Piezoelectric and Thermoelectric Energy Simultaneous Extraction Interface Circuit Based on Double Stack Resonance
来源出版物: IEEE TRANSACTIONS ON INDUSTRIAL ELECTRONICS 卷: 67 期: 6 页: 4567-4577 DOI: 10.1109/TIE.2019.2926047 出版年: 2020 出版日期: JUN
语种: English
文献类型: Article
作者关键词: Energy harvesting; Inductors; Integrated circuit modeling; Power generation; RLC circuits; Parasitic capacitance; Switching circuits; Double stack resonance; energy harvesting; piezoelectric transducer (PZT); self-powered; thermoelectric generator (TEG)
KeyWords Plus: HARVESTING CIRCUIT; VIBRATION; MANAGEMENT; RECTIFIER; SOLAR
作者地址: [Wang, Xiudeng; Xia, Yinshui; Xia, Huakang; Ye, Yidie; Chen, Zhidong] Ningbo Univ, Fac Elect Engn & Comp Sci, Ningbo 315211, Peoples R China.
[Shi, Ge] China Jiliang Univ, Coll Mech & Elect Engn, Hangzhou 310018, Peoples R China.
通讯作者地址: Wang, XD (reprint author), Ningbo Univ, Fac Elect Engn & Comp Sci, Ningbo 315211, Peoples R China.
电子邮件地址: 1611082572@nbu.edu.cn; xiayinshui@nbu.edu.cn; shige@cjlu.edu.cn; xiahuakang@nbu.edu.cn; yeyidie@nbu.edu.cn; 1701082016@nbu.edu.cn
ORCID 号: Wang, Xiudeng/0000-0002-5014-6038
引用的参考文献数: 33
核心合集中的 "被引频次": 0
被引频次合计: 0
出版商: IEEE-INST ELECTRICAL ELECTRONICS ENGINEERS INC
出版商所在城市: PISCATAWAY
出版商地址: 445 HOES LANE, PISCATAWAY, NJ 08855-4141 USA
ISSN: 0278-0046
eISSN: 1557-9948
长度为 29 个字符的来源文献名称缩写: IEEE T IND ELECTRON
ISO 来源文献名称缩写: IEEE Trans. Ind. Electron.
来源出版物页码计数: 11
Web of Science 学科分类: Automation & Control Systems; Engineering, Electrical & Electronic; Instruments & Instrumentation
Web of Science 研究方向: Automation & Control Systems; Engineering; Instruments & Instrumentation
IDS 号: KX5ZL
入藏号: WOS:000521959100030
输出日期: 2020-06-02

检索人员：赖悦君

教育部科技查新工作站（Z19）

2020年6月2日

证书号第4622420号

发明专利证书

发明名称：一种压电与光能协同采集电路

发明人：夏银水;王修登

专利号：ZL 2020 1 0680786.1

专利申请日：2020年07月15日

专利权人：宁波大学

地址：315211 浙江省宁波市江北区风华路818号

授权公告日：2021年08月17日　　授权公告号：CN 112003496 B

国家知识产权局依照中华人民共和国专利法进行审查，决定授予专利权，颁发发明专利证书并在专利登记簿上予以登记。专利权自授权公告之日起生效。专利权期限为二十年，自申请日起算。

专利证书记载专利权登记时的法律状况。专利权的转移、质押、无效、终止、恢复和专利权人的姓名或名称、国籍、地址变更等事项记载在专利登记簿上。

局长
申长雨

国家知识产权局
2021年08月17日

其他事项参见续页

证书号第4778212号

国家税务总局北京市海淀区税务局 印花税 代扣专用章 国家知识产权局

专利权人应当依照专利法及其实施细则规定缴纳年费。本专利的年费应当在每年07月29日前缴纳。未按照规定缴纳年费的，专利权自应当缴纳年费期满之日起终止。

申请日时本专利记载的申请人、发明人信息如下：

申请人：

宁波大学

发明人：

夏银水；王修登；沈家辉；王家欢

国家奖学金荣誉证书

编号：　BSY202108473

59

王修登　同学荣获2021年博士研究生国家奖学金，特颁此证。

中华人民共和国教育部

2021年12月31日

国家奖学金荣誉证书

编号：BSY202008522

09

王修登 同学荣获2020年博士研究生国家奖学金，特颁此证。

中华人民共和国教育部

2020年12月31日